

Activation of cell surface GRP78 decreases endoplasmic reticulum stress and neuronal death

Morgane Louessard¹, Isabelle Bardou¹, Eloïse Lemarchand¹, Audrey M Thiebaut¹, Jérôme Parcq¹, Jérôme Leprince², Anne Terrisse³, Valérie Carraro³, Pierre Fafournoux³, Alain Bruhat³, Cyrille Orset¹, Denis Vivien^{1,4}, Carine Ali¹ and Benoit D Roussel^{*,1}

The unfolded protein response (UPR) is an endoplasmic reticulum (ER) -related stress conserved pathway that aims to protect cells from being overwhelmed. However, when prolonged, UPR activation converts to a death signal, which relies on its PERK-eIF2 α branch. Overactivation of the UPR has been implicated in many neurological diseases, including cerebral ischaemia. Here, by using an *in vivo* thromboembolic model of stroke on transgenic ER stress-reporter mice and neuronal *in vitro* models of ischaemia, we demonstrate that ischaemic stress leads to the deleterious activation of the PERK branch of the UPR. Moreover, we show that the serine protease tissue-type plasminogen activator (tPA) can bind to cell surface Grp78 (78 kD glucose-regulated protein), leading to a decrease of the PERK pathway activation, thus a decrease of the deleterious factor CHOP, and finally promotes neuroprotection. Altogether, this work highlights a new role and a therapeutic potential of the chaperone protein Grp78 as a membrane receptor of tPA capable to prevent from ER stress overactivation.

Cell Death and Differentiation (2017) 24, 1518–1529; doi:10.1038/cdd.2017.35; published online 23 June 2017

The endoplasmic reticulum (ER) stress is a conserved cellular process that activates the unfolded protein response (UPR) that controls the correct functioning of the ER.¹ The UPR combines two responses: an early inhibition of protein synthesis, to avoid protein overload within the ER; and a later upregulation of genes that help protein folding, to clear the ER from native/aberrant proteins.² If prolonged, the UPR triggers death signals.³

Three sensors present at the ER membrane ensure a correct detection of ER stress: IRE1 (inositol-requiring protein-1); ATF6 (activating transcription factor 6); and PERK (protein kinase RNA (PKR)-like ER kinase). IRE1 and ATF6 are normally bound to, and thus inactivated by the ER chaperone Grp78 (78 kDa glucose-related protein, also called Bip for binding immunoglobulin protein). Under stress conditions, Grp78 disengages from IRE1 and ATF6, leading to their activation and the subsequent expression of UPR genes (chaperones, folding and ER proteins).⁴ Like the other two sensors, PERK is held inactive by the binding of Grp78. Under stress conditions, PERK phosphorylates its unique substrate, eIF2 α (eukaryotic translation initiation factor-2 α -subunit),⁵ resulting in a global protein synthesis shutdown.⁶ Paradoxically, PERK-mediated eIF2 α phosphorylation also activates the transcription of specific genes, including ATF4 (activating transcription factor 4), which triggers a transcriptional programme of stress-responsive genes⁷ and of the transcription factor CHOP (C/EBP homologous protein); in case of ER stress overactivation, CHOP will induce death signals.⁸ Another target of ATF4 and CHOP, GADD34 (growth arrest and DNA damage-inducible protein 34, a protein phosphatase

1 regulatory subunit), serves as a negative feedback loop by dephosphorylating eIF2 α , allowing the recovery of protein translation⁴ (Figure 1a).

These molecular events have been implicated in many neurological diseases, including Alzheimer's disease, Parkinson's disease, Huntington's disease and stroke.^{4,9} Many stroke models are known to activate the UPR.^{10,11} This activation is likely due to the energetic failure and the attendant dysfunctions of calcium pumps, ER-calcium depletion, chaperone dysfunction and the eventual accumulation of misfolded proteins.^{4,12} For example, activation of the PERK branch is evidenced by eIF2 α phosphorylation in a model of hypoxia/ischaemia in mice.¹³ Moreover, CHOP and GADD34 – the downstream targets of phosphorylated eIF2 α (phospho-eIF2 α) – are also increased during cerebral ischaemia.^{14–17}

In our study, we investigated ER stress-induced neuronal death by using an *in vivo* model of stroke and two different models of ischaemia/reoxygenation (*ex vivo* and *in vitro*). We demonstrate that the PERK branch of the UPR can be controlled by the activation of translocated-ER-resident chaperone Grp78 to the neuronal surface by tissue-type plasminogen activator (tPA). Binding of tPA to Grp78 results in a decrease of PERK/eIF2 α activation, and thus a decrease of the deleterious factor CHOP, leading to neuroprotection. For the first time, we describe an active role of cell surface Grp78 signalling in the control of ER stress, thus opening new therapeutic strategies for neurological diseases, especially during stroke.

¹Normandie Univ, UNICAEN, INSERM, Physiopathology and Imaging of Neurological Disorders, Caen, France; ²Normandie Univ, UNIROUEN, INSERM, Laboratoire Différenciation et Communication Neuronale et Neuroendocrine, Plate-forme de Recherche en Imagerie Cellulaire de Normandie (PRIMACEN), Rouen, France; ³INRA, UMR 1019 Nutrition Humaine, Centre de Clermont-Ferrand-Theix, Saint Genès Champanelle, France and ⁴Clinical Research Department, Medical Center, University Caen Normandy, Centre Hospitalo-Universitaire Caen Côte de Nacre, Caen, France

*Corresponding author: BD Roussel, GIP Cyceron-Caen Basse-Normandie University, INSERM U919, GIP Cyceron, Boulevard Becquerel, BP5229, Caen 14074, France. Tel: +33 2 31470213; Fax: +33 2 31470222; E-mail: broussel@cyceron.fr

Received 26.12.16; revised 20.2.17; accepted 23.2.17; Edited by N Bazan; published online 23.6.17

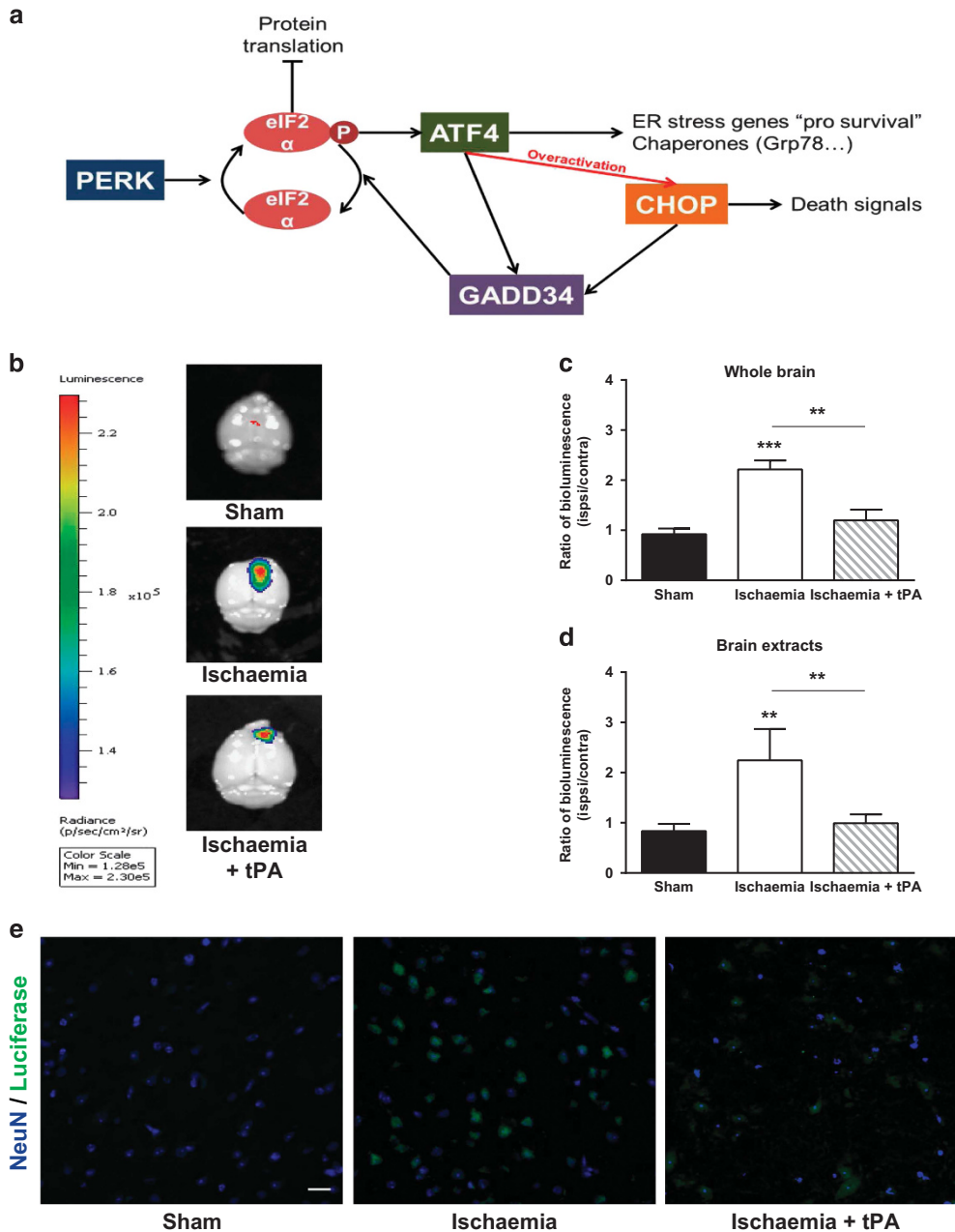


Figure 1 tPA protects neurons from ischaemia-induced ER stress in a thromboembolic model of stroke. (a) Diagram of the PERK branch of the UPR: PERK is an ER membrane-bound sensor activated under stress conditions. Once activated, it phosphorylates eIF2 α leading to a global shutdown in protein translation. Paradoxically, phospho-eIF2 α promotes ATF4 expression and subsequent protein-folding genes to restore ER homeostasis, including GADD34 to restore protein synthesis by dephosphorylating eIF2 α . If ER stress is over-activated, ATF4 leads to the expression of CHOP, partially responsible of ER stress-mediated death. (b) Representative cerebral bioluminescence intensities following sham surgery, thromboembolic ischaemia alone or coupled to thrombolysis with tPA (10 mg/kg IV) ($n=9$ for sham animals and $n=10$ for ischaemia and ischaemia+tPA). (c) Mean ipsilateral/contralateral hemispheres *ex vivo* bioluminescence ($n=9$ for sham animals and $n=10$ for ischaemia and ischaemia+tPA). (d) Mean ipsilateral/contralateral cortical lysates bioluminescence (data are represented as mean \pm S.E.M.; $n=9$ for sham animals and $n=10$ for ischaemia and ischaemia+tPA). (e) Representative immunostainings against luciferase (green) and NeuN (blue) in the peri-infarct area. (* $P<0.05$, ** $P<0.01$, *** $P<0.001$; Mann-Whitney test; scale bar, 20 μ m)

Results

Thromboembolic ischaemia induces activation of PERK/ATF4 branch of ER stress and is decreased by thrombolysis. CARE-Luciferase mice allow an *in vivo* detection of the activation of the PERK-eIF2 α branch of the UPR¹⁸ (Figure 1a). CARE-Luciferase mice were subjected to

thromboembolic stroke, induced by the injection of thrombin within the middle cerebral artery.¹⁹ This model allows thrombolysis by recombinant tPA in the same conditions than its use in clinic: a group of mice were thrombolysed with tPA 20 min after stroke induction (10 mg/kg iv; bolus and then infusion over 40 min) while sham group received saline. After 24 h, mice were perfused and brain were harvested to

measure *ex vivo* luciferase activity in the ischaemic (ipsilateral) and contralateral hemispheres. As shown on the images and on the quantifications (Figure 1b and c), ischaemic stroke increased by 2.4-fold the bioluminescent signal compared to sham conditions (ipsi/contralateral hemispheres) ($n=9$, $P<0.001$). Thrombolysis with tPA reduced by 46% ischaemia-induced luciferase signal ($n=9$; $P<0.01$). Concordant with the *ex vivo* findings, *in vitro* luciferase assays (Figure 1d) showed a strong ischaemia-induced luciferase activity (+270% versus sham mice; $n=9$; $P<0.01$) that was reduced by tPA-induced thrombolysis (56% reduction compared to ischaemia alone; $n=9$, $P<0.01$). Immunostainings against luciferase also highlighted in the peri-infarct cortical region a strong ischaemia-induced labelling which was reduced by thrombolysis (Figure 1e). However, because tPA can positively or negatively control neuronal survival through multiple pathways^{20,21} in addition to its thrombolytic effects, we wondered if the decrease of ER stress observed after thrombolysis was only due to its vascular properties or not.

OGD/reoxygenation induces a deleterious activation of the PERK branch of ER stress that is counteracted by tPA. tPA is now considered as a neuromodulator.^{20,22} Because it is complicated to decipher its parenchymal roles from its thrombolytic action, we decided to use a model of ischaemia where thrombolysis is not necessary: an *ex vivo* model of hippocampal slices subjected to 40 min of OGD followed by reoxygenation (OGD_{reox}) (Figure 2a). To ensure ER stress activation, we measured the level of eIF2 α phosphorylation by western blots 24 h after the experiment. When compared to control, OGD_{reox} led to an increase of eIF2 α phosphorylation (Figure 2b and quantification in Figure 2c, 2.5-fold increase, $P<0.01$), confirming the activation of ER stress. Interestingly, tPA prevented OGD_{reox}-mediated eIF2 α phosphorylation (Figure 2d and quantification in Figure 2c, $n=6$, $P<0.05$) independently from its thrombolytic properties. We also assessed cell death, by propidium iodide staining (Figure 2d) and as observed *in vivo* after ischaemic stroke, tPA protected from OGD_{reox}-induced cell death (Figure 2e, 60% of protection, $n=5$, $P<0.01$). Taken together, these results show that during OGD_{reox}, tPA reduces the activation of the PERK-eIF2 α branch of the UPR independently of its thrombolytic activity.

OGD/reoxygenation overactivates the PERK branch of ER stress in pure cortical neurones and is decreased by tPA. To study the mechanism of action of tPA, we next used cultures of pure cortical neurones subjected to OGD_{reox} (Figure 3a). In these conditions, the PERK-eIF2 α branch was activated, as illustrated by immunostainings against phospho-eIF2 α (Figure 3b). ER stress activation increased as a function of the duration of OGD, as shown by the extent of eIF2 α phosphorylation ratio compared to the total form, after various time of OGD and followed by 4 h of reoxygenation (Figure 3c and densitometries in Figure 3d, 1.84-, 2.68- and 3.86-fold increase of eIF2 α phosphorylation at 10, 40 and 60 min of OGD, respectively, $P<0.05$). In this neuronal model, tPA 300 nM also prevented the activation of the PERK branch as illustrated by immunostainings (Figure 3b) and immunoblots against phospho-eIF2 α (Figure 3c and

densitometries in Figure 3d, tPA reduces by 44%, 46% and 40% the phosphorylation of eIF2 α after 10, 40 and 60 min of OGD_{reox}, respectively, $P<0.05$). We also studied by qPCR the transcriptional downstream targets of phospho-eIF2 α (Figure 1a). OGD_{reox} increased mRNA levels of ATF4, CHOP, GADD34 and Grp78 (Figure 3e) by 2-, 1.6-, 1.54- and 1.6-fold, respectively. This ER stress activation measured by qPCR was totally prevented in the presence of tPA, except for Grp78 (Figure 3e). In parallel to these evidence of time-dependent activation of the PERK-eIF2 α branch, we also found that OGD_{reox} induced a neuronal death of which the extent increased with the duration of OGD (Supplementary Figure 1; Spearman correlation test: $\rho=0.777$; $P<0.0001$) and that was correlated to the levels of phospho-eIF2 α (Spearman correlation test: $\rho=0.671$; $P=0.026$). Co-treatment with tPA (300 nM) reduced by 38% the extent of neuronal loss induced by OGD_{reox} (40 min OGD followed by 4 h reoxygenation; Figure 3f, $P<0.01$), showing a neuroprotective action of tPA via an alleviation of the recruitment of the PERK branch of the UPR in ischaemic neurones.

The neuronal ER continuity is preserved under OGD/reoxygenation in the presence of tPA. ER dysfunction is often associated to ER swelling and fragmentation. To visualize the neuronal ER continuity/integrity in our experimental conditions, we performed live imaging of neurones with the cell-permeant dye ER tracker (Figure 4). Due to the use of glass bottom Petri dishes for the confocal acquisition, neurones need the presence of astrocytes to attach to the glass bottom part; we then adapted the protocol of OGD_{reox} to 1 h of OGD, in order to obtain the same level of cell death than 40 min OGD on pure cortical neurones. Z-stack acquisitions were performed to enable a 3D reconstruction by Imaris Software (Bitplane; Concord, MA, USA) (representative reconstruction Figure 4a, blue images). In control conditions (with or without 300 nM tPA), the ER continuity was preserved with an ER surrounding the nucleus and projecting in neurites (Figure 4a). However, after OGD_{reox} the ER continuity was lost, with an apparent swelling and an ER fragmentation (Figure 4a, blue images). When tPA was added during the OGD_{reox}, ER continuity was preserved. Neuronal swelling was estimated by measuring the somatic diameter of neurones (10 per condition, in five distinct microscopic fields; each individual neurones was recorded every hour) after staining with the ER tracker as illustrated on the images at 4 h (Figure 4a, green images). Under control conditions, tPA 300 nM alone did not modify the neuronal body diameter, while OGD_{reox} led to a 1.5-, 1.8-, 2.11-, 2.26- and 2.34-fold increase of neuronal body diameter at t0, t1, t2, t3 and t4 respectively, $***P<0.001$ compared to control). When tPA is added during OGD_{reox}, the neuronal body diameter increased over time (Figure 4b, 1.05-, 1.1-, 1.16- and 1.18-fold at t0, t1, t2, t3 and t4 respectively; $**P<0.01$, $***P<0.001$ compared to control) but less than under OGD_{reox} alone (Figure 4b, 31%, 29%, 22%, 23% less than OGD_{reox} at t0, t1, t2, t3 and t4, respectively; $P<0.001$ compared to OGD_{reox} alone). It demonstrates that tPA is able to maintain ER continuity and the neuronal morphology under OGD_{reox}.

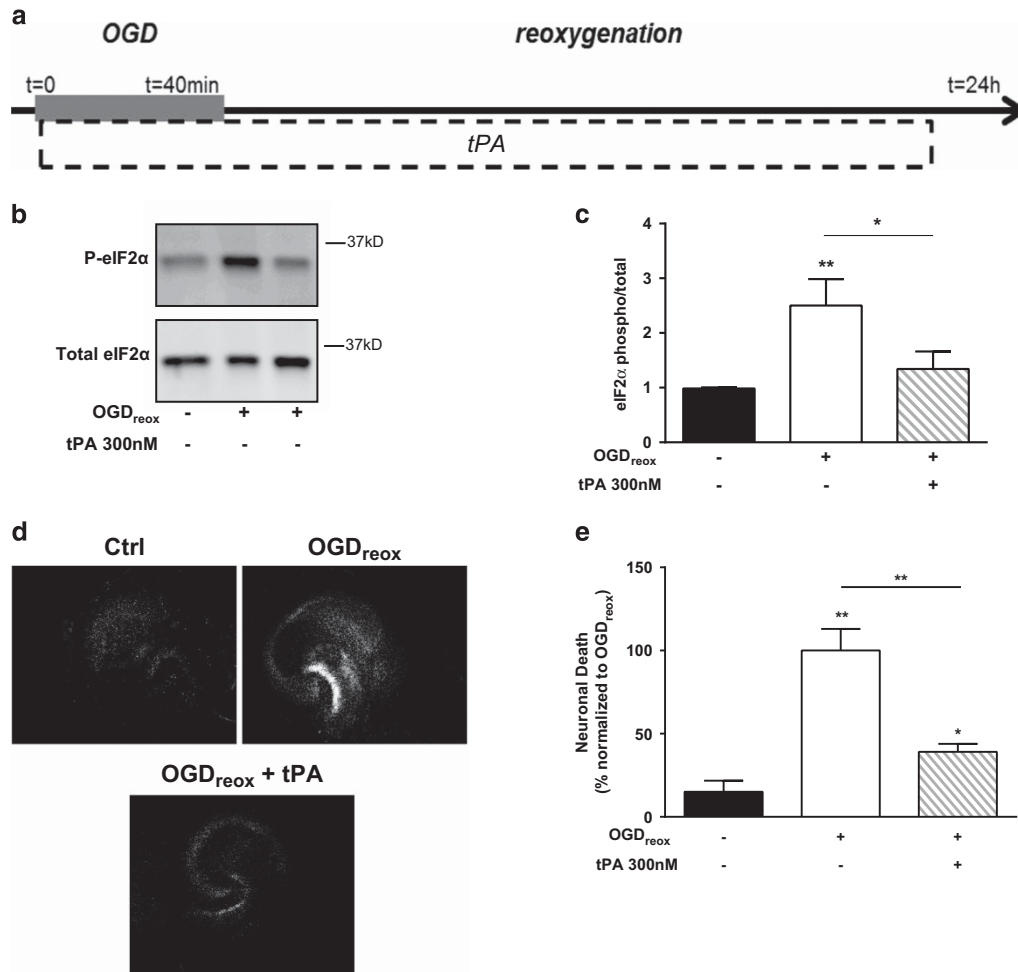


Figure 2 tPA protects hippocampal slices from OGD_{reox}-induced death by decreasing the PERK branch of the UPR. (a) Diagram of the OGD_{reox} protocol used on hippocampal slices. Slices were washed with OGD media and stayed under OGD conditions during 40 min, followed by a 24 h reoxygenation period. (b) Representative western blots against phosphor- and total eIF2 α in hippocampal slices subjected or not to OGD_{reox} \pm 300 nM tPA. (c) Corresponding ratio of the phosphorylated versus total form of eIF2 α (data are represented as mean \pm S.E.M. $n=6$, * $P<0.05$; ** $P<0.01$; Mann-Whitney test). (d) Representative propidium iodide stainings of slices 24 h after 40 min of OGD (except Ctrl) in presence or not of 300 nM tPA (Scale bar, 10 μ M). (e) Mean of propidium iodide-positive cells in slices 24 h after treatments and normalized to the OGD_{reox} condition (data are represented as mean \pm S.E.M. $n=5$ independent experiments; * $P<0.05$; ** $P<0.01$; Mann-Whitney test)

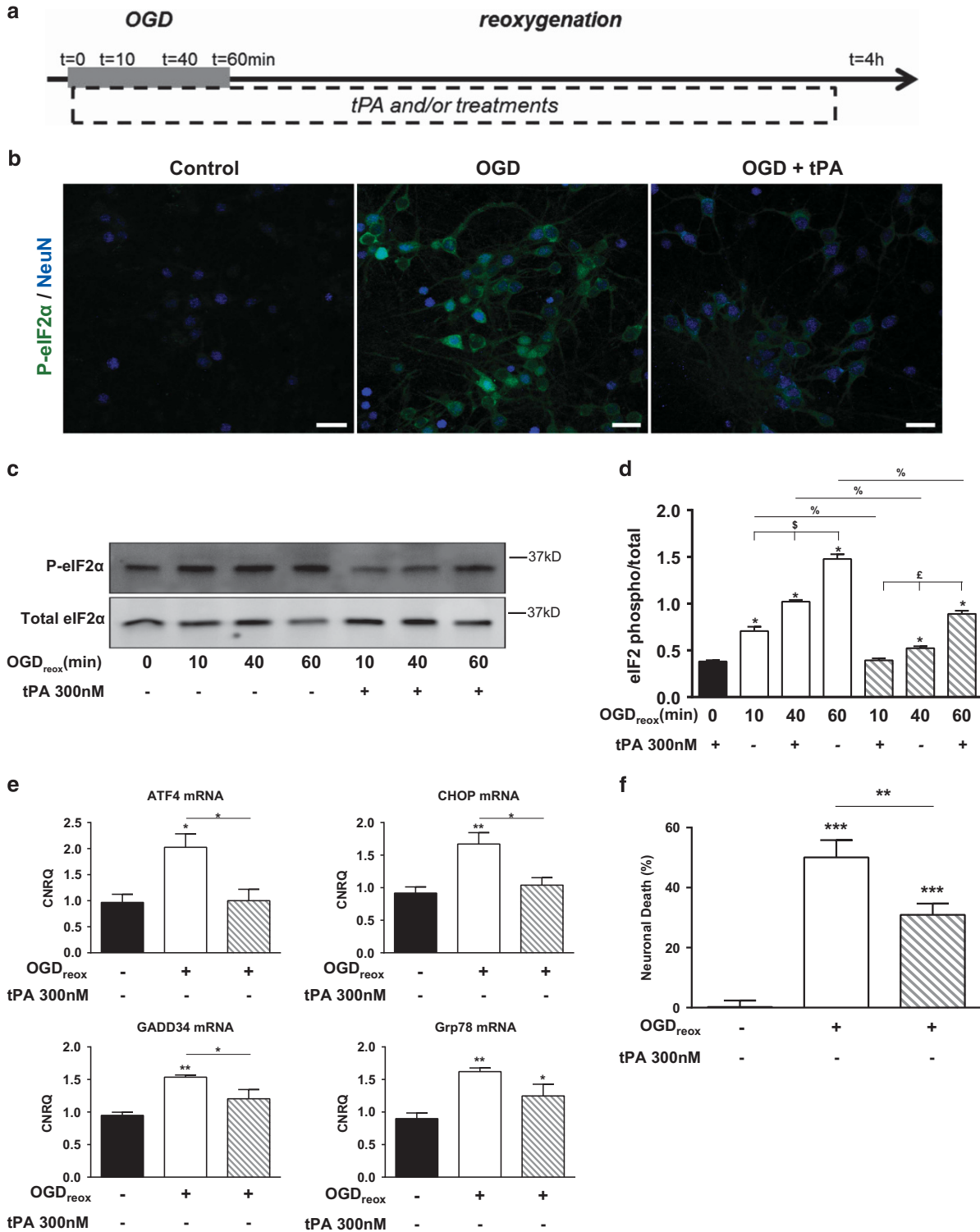
tPA decreases the PERK-eIF2 α branch of the UPR by a mechanism dependent on its lysine-binding site. We then investigated the mechanisms by which tPA decreases the PERK branch of ER stress and death under OGD_{reox}. We first used a proteolytically inactive form of tPA (itPA: tPA-dGGACK; 300 nM) and showed that despite its lack of enzymatic activity, itPA remained able to confer neuroprotection (Figure 5a, 19% of neuronal death for itPA under OGD_{reox}; 50% for OGD_{reox} alone; and 31% for tPA and OGD_{reox}, $P<0.001$). The growth factor domain of tPA confers anti-apoptotic capacity through its binding to the EGF receptor.^{23,24} However, AG1478 (5 μ M), an EGFR tyrosine kinase inhibitor, did not prevent the beneficial effect of tPA during OGD_{reox} (Figure 5b, 31% of neuronal death for tPA under OGD_{reox}; 26% for tPA+AG1478 under OGD_{reox}), excluding a role for EGF receptor. tPA can also interact through its finger domain with LRP-1 (type 1 low-density lipoprotein receptor-related protein) to promote NF κ B activation²⁵ and Akt phosphorylation.²⁶ The addition of RAP

(receptor-associated protein) (500 nM), a competitive LRP-1 antagonist, did not reverse the protective effect of tPA (Figure 5c, 31% of neuronal death for tPA under OGD_{reox}; 38% for tPA+RAP under OGD_{reox}). The lysine-binding site (LBS) contained in the Kringle 2 domain of tPA is involved in the interaction of tPA with several partners (for review ref. 22). In order to compete with the binding of its LBS, we used the lysine analogue TXA (tranexamic acid) at the same concentration than tPA (300 nM). Interestingly, TXA reversed the protective effect of tPA during OGD_{reox} (Figure 5d, 27% of neuronal death for tPA under OGD_{reox}; 41% for tPA+TXA under OGD_{reox}, $P<0.05$), suggesting a role for the LBS contained within the Kringle 2 domain of tPA to mediate its action on neuroprotection during OGD_{reox}.

OGD/reoxygenation promotes cell surface Grp78, and its activation induces a beneficial decrease of ER stress. It is now well accepted that under ER stress conditions, the ER-resident chaperone Grp78 translocates to the cell

surface.^{27,28} To confirm this in our OGD_{reox} conditions, we biotinylated membrane proteins before and after 40 min of OGD, and we performed an avidin pull-down followed by a western blotting against Grp78. We show an increase of cell surface Grp78 after OGD compared to control (Figure 6a), in favour of a translocation of Grp78 to the neuronal membrane.

We then checked the ability of tPA to be a cell surface Grp78 ligand. Immunoprecipitations (IP) were performed with both Grp78 and tPA antibodies on neurons subjected to OGD_{reox} and treated or not with 300 nM of tPA (Figure 6b). The pull-down with Grp78 antibodies revealed a Grp78 band by western blot as a positive control, and the tPA pull-down also



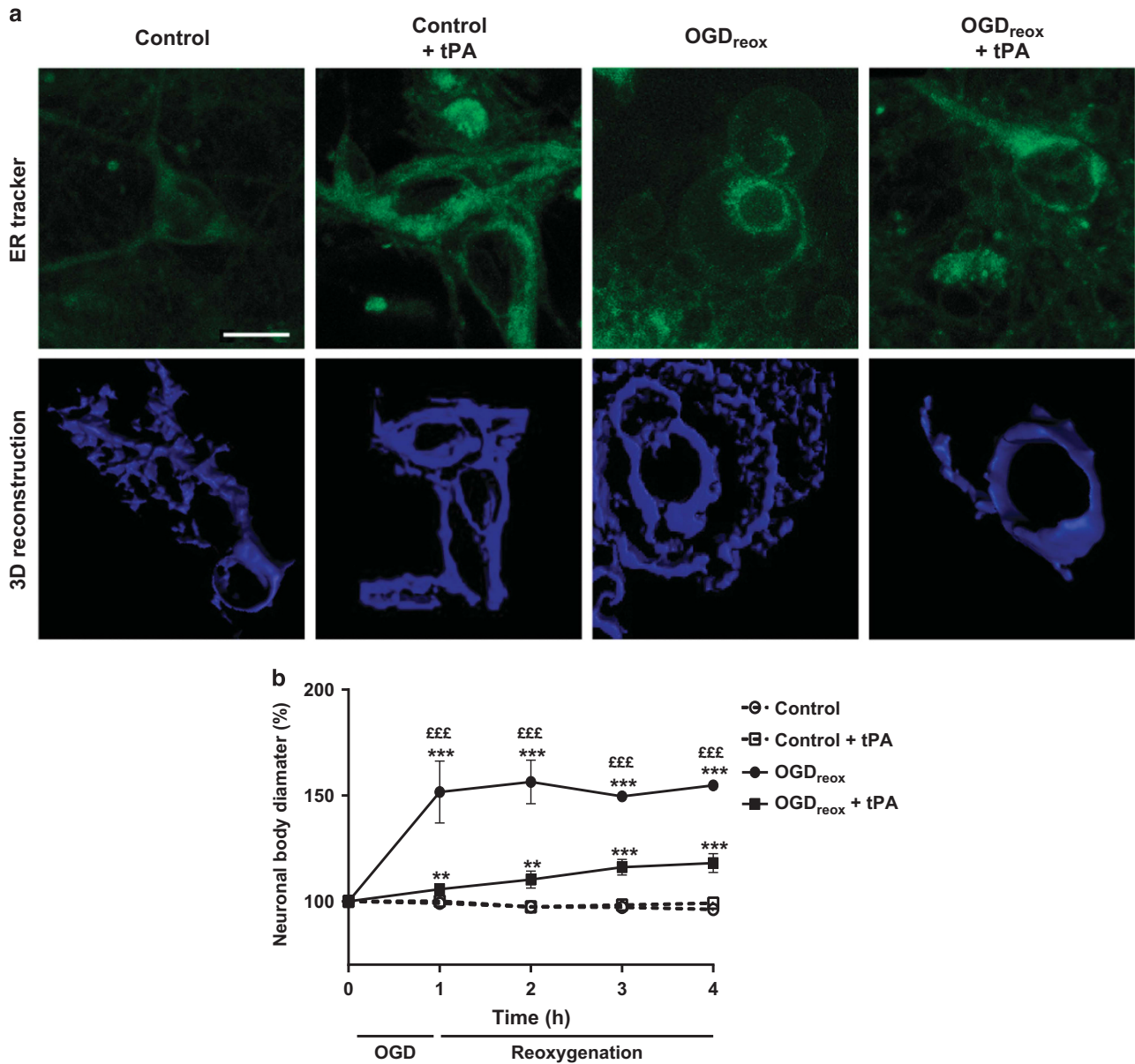


Figure 4 tPA preserves ER neuronal continuity after OGD_{reox}. (a) Representative pictures of neurones labelled with ER-tracker (in green) and 3D construction (in blue) after OGD_{reox} (1 h OGD+4 h of reoxygenation) or not and in the presence or not of 300 nM tPA (scale bars, 5 μ M). (b) Neuronal body diameter at different time (before OGD: t0; after 1 h of OGD: t1; and after 1 h: t2, 2 h: t3 and 3 h: t4 of reoxygenation) in presence or not of 300 nM tPA (data are represented as mean \pm S.E.M. $n=9$ independent experiments with 10 neurones counted in five different areas for each experiment and each time point; ** $P<0.01$; *** $P<0.001$; compared with control or control-tPA condition; ^{£££} $P<0.001$; compared with OGD-tPA condition; Mann–Whitney tests)

Figure 3 tPA decreases the PERK branch of the UPR-mediated neuronal death under OGD_{reox} conditions. (a) Diagram of the OGD_{reox} protocol used on pure cortical neurones. Neurones were washed with OGD media and stayed under OGD conditions during 40 min followed by a 4 h reoxygenation period. (b) Representative immunostainings against phospho-eIF2 α (in green) and NeuN (in blue) on cultured neurones subjected or not to 40 min of OGD \pm 300 nM tPA (representative images of three independent experiments; scale bar, 20 μ m). (c) Representative western blots against phospho- and total eIF2 α after various time of OGD (10, 40 and 60 min) followed by 4 h of reoxygenation, in the presence or not of 300 nM tPA. (d) Corresponding ratio of the phosphorylated versus total form of eIF2 α (data are represented as mean \pm S.E.M. $n=5$; * $P<0.05$ versus Ctrl condition; [§] $P<0.05$ between OGDreox conditions; [£] $P<0.05$ between OGDreox+tPA conditions; [¶] $P<0.05$ between OGDreox versus OGDreox+tPA conditions; Mann–Whitney test). (e) qPCR analyses of ATF4, CHOP, GADD34 and Grp78 after OGD_{reox} in the presence or not of 300 nM tPA (data are represented as mean \pm S.E.M. $n=5$; * $P<0.05$; ** $P<0.01$; Mann and Whitney test; CNRQ: calibrated normalized relative quantities). (f) Neuronal death assessed by LDH release after OGD_{reox} in the presence or not of 300 nM tPA (data are represented as mean \pm S.E.M. Ctrl: $n=32$; OGD: $n=28$; OGD+tPA: $n=32$; from four independent experiments. ** $P<0.01$; *** $P<0.001$; Mann–Whitney test)

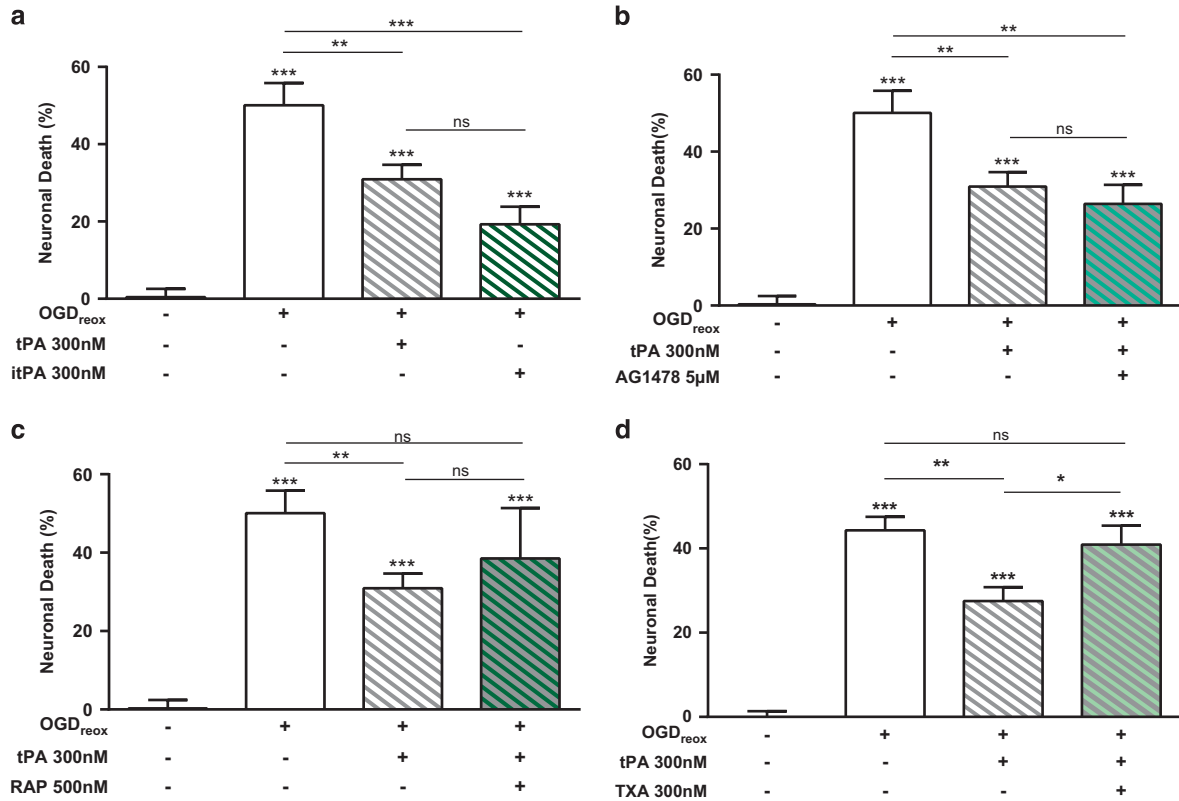


Figure 5 the LBS contained within the kringle 2 domain of tPA is involved in the decrease of the PERK branch of the UPR-mediated neuronal death during OGD_{reox}. (a) Neuronal death assessed by LDH release in the media after 40 min of OGD followed by 4 h of reoxygenation in the presence or not of 300 nM tPA, or in the presence of inactive tPA (itPA) 300 nM. tPA was also tested in addition to AG1478 5 µM (b), RAP (500 nM) (c) and TXA 300 nM (d), (data are represented as mean ± S.E.M. *n* = 30 for ctrl, *n* = 28 for OGD, *n* = 32 for tPA, *n* = 22 for itPA, *n* = 18 for AG1478, *n* = 12 for RAP, *n* = 16 for TXA; from four independent experiments; **P* < 0.05; ***P* < 0.01; ****P* < 0.001; Mann-Whitney test)

revealed a Grp78 band (Figure 6b), confirming tPA as a ligand. Indeed, the interaction between tPA and cell surface Grp78 has been reported in neuroblastoma cells.²⁹ The binding of tPA to Grp78 occurs on the amino acid sequence 98–115 (LIGRTWNDPSVQQDIKFL).²⁹ We thus synthesized a corresponding competitive peptide called Grp78_(98–115), and confirmed its competitive nature in a plasminogen-like fluorogenic substrate assay. Recombinant Grp78 7.3 pM (equimolar to tPA concentration) or 10 times concentrated increased tPA fibrinolytic activity by 25 and 40% respectively (Supplementary Figure 2A, *P* < 0.001). Interestingly, a tPA mutated in its LBS contained within the kringle 2 domain (tPA K2*: W253R mutation) is no longer able to interact with Grp78, as shown by the absence of increased tPA K2* activity (Supplementary Figure 2B). When co-incubated with Grp78_(98–115) (7.3 or 73 pM), Grp78 could no longer potentiate tPA fibrinolytic activity (Supplementary Figure 2A). A scramble peptide Grp78_{(98–115)sc} had no action on the potentiation of tPA fibrinolytic activity by Grp78 (Supplementary Figure 2A; *P* < 0.01). We then ensured the capacity of Grp78_(98–115) to decrease the binding of tPA to cell surface Grp78 in living neurones. ³⁵S radiolabelled tPA (tPA*) was incubated on neurones after 40 min of OGD in the presence or not of Grp78_(98–115) (10 µM) during 30 min at 4 °C (to avoid any active process of internalization). Our data demonstrate a

decrease of tPA* at the neuronal membrane in the presence of Grp78_(98–115) (Figure 6c, 49.2% decreased with Grp78_(98–115); *P* < 0.001), confirming the ability of our peptide to decrease the binding between tPA and cell surface Grp78 in neurones. We then tested the blocking peptide under OGD_{reox} conditions. After 40 min of OGD and 4 h of reoxygenation, Grp78_(98–115) reversed tPA-mediated inhibition of the PERK branch, as shown by western blot against eIF2α phosphorylation (Figure 6d) and the corresponding densitometries (Figure 6e; ratio of 1.02 between the phosphorylated and the total form of eIF2α for tPA under OGD_{reox}; 1.52 for tPA + Grp78_(98–115) under OGD_{reox}; *P* < 0.05). Interestingly, Grp78_(98–115) totally reversed the neuroprotective effect of tPA in cortical neurones (Figure 6f, 31% of neuronal death for tPA + Grp78_(98–115) under OGD_{reox}, 12% for tPA under OGD_{reox}; *P* < 0.01). To ensure our findings, we also tried the peptide on hippocampal slices subjected to OGD_{reox}. Grp78_(98–115) also reversed tPA-mediated inhibition of the PERK branch as shown by western blot against eIF2α phosphorylation (Figure 6g and the densitometries Figure 6h; ratio of 1.02 between the phosphorylated and the total form of eIF2α for tPA under OGD_{reox}; 1.52 for tPA + Grp78_(98–115) under OGD_{reox}; *P* < 0.05). Grp78_(98–115) also prevented the protection by tPA on hippocampal slices subjected to OGD_{reox} (Figure 6i, 61% of protection for tPA under OGD_{reox},

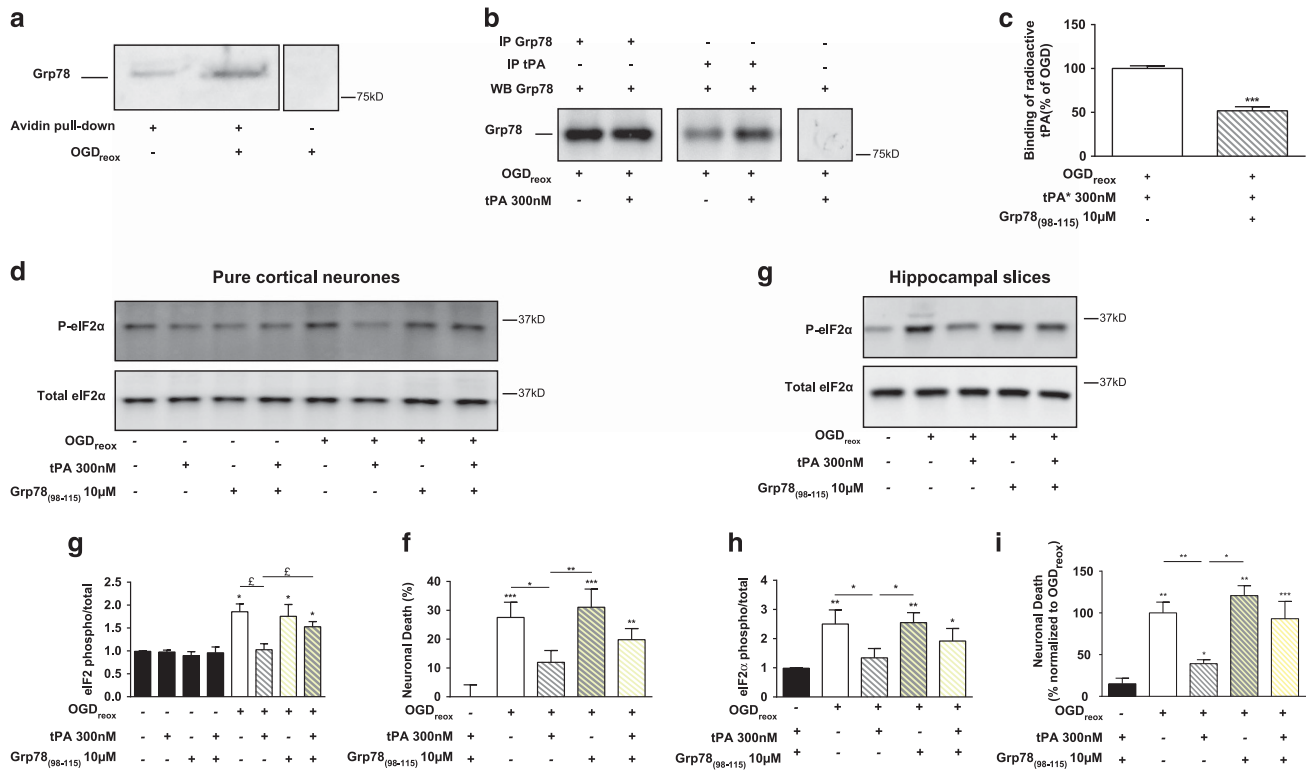


Figure 6 The interaction between tPA and cell surface Grp78 is responsible of the decrease of the PERK branch activation and the associated neuroprotection during OGD_{reox}. (a) Avidin pull-down and western blot against Grp78 on neurones subjected or not to 40 min of OGD, followed by the biotinylation of membrane protein at 4 °C (representative blot from $n = 3$ independent experiments). (b) Immunoprecipitations with either Grp78 or tPA antibodies on neurones subjected to 40 min of OGD, and revealed by western blot against Grp78 (representative blot of three independent experiments). (c) Membrane-bound radioactivity after radioactive tPA (tPA*) incubation (30 min) at 4 °C following a 40 min OGD period in presence or not of 10 μM of Grp78₍₉₈₋₁₁₅₎ peptide (data are represented as mean Immunoprecipitation ± SEM $n = 4$ independent experiments; *** $P < 0.001$ Mann–Whitney test). (d) Representative western blots against phospho- and total eIF2α and corresponding densitometries (e) from pure cortical neurones subjected to 40 min of OGD followed by 4 h of reoxygenation, in the presence or not of 300 nM tPA and 10 μM Grp78₍₉₈₋₁₁₅₎ (data are represented as mean ± S.E.M. $n = 5$ independent experiments; * $P < 0.05$ compared to normoxia; [†] $P < 0.05$ compared between OGD_{reox} conditions). (f) Neuronal death of pure cortical neurones assessed by LDH release after 40 min of OGD followed by 4 h of reoxygenation in the presence or not of 300 nM tPA and 10 μM Grp78₍₉₈₋₁₁₅₎ (data are represented as mean ± S.E.M. $n = 25$ for ctrl, $n = 20$ for OGD_{reox}, $n = 16$ for tPA, tPA+Grp78₍₉₈₋₁₁₅₎ and Grp78₍₉₈₋₁₁₅₎ from five independent experiments; * $P < 0.05$; ** $P < 0.01$; *** $P < 0.001$; Mann–Whitney test). (g) Representative western blots against phospho- and total eIF2α on hippocampal slices subjected to 40 min of OGD followed by 24 h of reoxygenation, in the presence or not of 300 nM tPA and 10 μM Grp78₍₉₈₋₁₁₅₎ and corresponding ratio of the phosphorylated versus total form of eIF2α (h) (data are represented as mean ± S.E.M. $n = 6$; * $P < 0.05$; ** $P < 0.01$; Mann–Whitney test). (i) Cell death assessed by counting of propidium iodide-positive cells in slices 24 h after treatments and normalized to the OGD_{reox} condition in the presence or not of 300 nM tPA and 10 μM Grp78₍₉₈₋₁₁₅₎ (data are represented as mean ± S.E.M. $n = 12$ from four independent experiments; * $P < 0.05$, ** $P < 0.01$, *** $P < 0.001$, Mann–Whitney test)

totally reversed with the co-application of Grp78₍₉₈₋₁₁₅₎, ** $P < 0.01$). Again, this effect was associated with a reversion of the inhibition of eIF2α phosphorylation by tPA (Figure 6g and h, ratio of 1.34 between the phosphorylated and the total form of eIF2α for tPA under OGD_{reox}, 2.55 for tPA+Grp78₍₉₈₋₁₁₅₎ under OGD_{reox}; $P < 0.05$). Taken together, these data show that modulating cell surface Grp78 during intense ER stress is a new and interesting therapeutic target to prevent cell death from deleterious ER stress.

Discussion

In this study, we demonstrate for the first time that the binding of tPA to cell surface Grp78, triggers a signal that decreases detrimental ER stress overactivation in neurones, resulting in neuroprotection. We also show that ischaemic events lead to the translocation of the chaperone Grp78 from the ER to the neuronal surface, a mechanism described under ER stress activation and in cancer.^{27,28} Interestingly, the serine protease

tPA is able to bind to cell surface Grp78 leading to a decrease of the PERK/eIF2α axis of the UPR, and resulting in neuronal survey during cerebral ischaemia.

To study ER stress activation, we first subjected CARE-luciferase mice to thromboembolic ischaemia, alone or coupled to reperfusion by tPA in the same conditions than its clinical use.¹⁹ We observed a strong activation of the eIF2α-ATF4 pathway after ischaemic stroke, a surrogate marker of the activation of the PERK-eIF2α branch of the UPR. Indeed, while kinases other than PERK can phosphorylate eIF2α (GCN2 (general control nonderepressible 2), HRI (haem-regulated eIF2α kinase) and PKR (Protein kinase RNA-activated), studies in genetically deficient mice revealed that during cerebral ischaemia, PERK is the only kinase responsible for eIF2α phosphorylation.^{30,31}

We also demonstrated an increase of cell surface Grp78 at the neuronal surface after OGD_{reox} (Figure 6a). Grp78 is mostly known as an ER chaperone, belonging to the heat-shock protein family, but it has also been described at the cell

surface of cancer cells,^{29,32} macrophages,²⁷ endothelial cells,^{33,34} and cardiomyocytes.³² Accordingly, Grp78 is now recognized as a receptor/co-receptor for different partners, including activated α 2-macroglobulin,³⁵ plasminogen/microplasminogen,³⁶ some viruses,^{37,38} major histocompatibility complex class I³⁸ and voltage-dependent anion channels.³⁶ Grp78 has also been shown to interact with tPA, resulting in an increase in plasmin formation.²⁹ Here, we demonstrate the presence of cell surface Grp78 in neurones, and we confirm the occurrence of the interaction between Grp78 and recombinant tPA (Figure 6b), but extend its functional impact to neuroprotection. To our knowledge, Grp78 has no intrinsic ability to convey intracellular signals, as demonstrated by analyses of its sequence and hydrophobicity.²⁷ Rather, Grp78 would need co-receptors.²⁷ In our study, none of the classical neuronal receptors of tPA (NMDA receptor, LRP1, EGFR) seem to be involved in the effect observed (Figure 5).

Hypoxia/ischaemia³⁹ or ER stress^{28,32} are known triggers of Grp78 translocation. However, how Grp78 translocates from the ER to the cell membrane remains unclear. In 293 T cells, thapsigargin treatment leads to a 12-fold increase of cell surface Grp78 that is different from its increase within the ER,³² suggesting that ER stress promotes specific mechanism(s) to enhance cell surface localization of Grp78. Importantly, Grp78 is brought to the cell surface by a specific mechanism, as extracellular Grp78 originating from dead cells cannot stably attach to the cell surface.³² In addition, a same signal induces or not Grp78 translocation in different cells. For instance, hypoxia enhances Grp78 at the membrane of neurones but not of astrocytes.³⁹

Our study also describes a new role for the serine protease tPA. It remains the gold standard treatment for cerebral ischaemia despite its short therapeutic window.^{40,41} But since several years, it is clearly admitted that tPA is more than a vascular enzyme with many roles in the cerebral physiology pathology.²⁰ tPA has first been described as a pro-excitotoxic protein,⁴² mainly by interacting with the GluN1 subunit of the NMDA receptor.⁴³ In the meantime, it has also been shown that cerebral tPA was anti-apoptotic.⁴⁴ Things seem more complex, as depending of its form, its dose, and its localization tPA can display pro-survival effects on neurones.^{21,45} For example, tPA is neuroprotective in a model of glucose privation⁴⁶ and a model of cerebral ischaemia,⁴⁷ and this effect required NMDA receptors. At the first look, it could seem contradictory with previous findings where tPA interaction with NMDA receptors was detrimental in stroke.^{43,48} But in fact it seems that protective effects of tPA are mediated by the activation of synaptic NMDA receptors,⁴⁷ while its activation of extrasynaptic receptors leads to excitotoxicity.⁴⁹ Here, we identified cell surface Grp78 as a new neuronal receptor of tPA. Its binding leads to negative feedback on the PERK branch activation, resulting in less eIF2 α phosphorylation, and more importantly less *CHOP* induction, so less death during ischaemic events. Importance of Grp78 is confirmed by studies using AdoPep1, a peptide identified in the metalloproteinase domain of a disintegrin and metalloproteinase 15 protein (ADAM15), that binds to cell surface Grp78 and inhibits hypoxia-induced apoptosis in endothelial cells and increases Akt phosphorylation and ERK 1/2 activation.³⁴ Moreover,

AdoPep1 also inhibits hypoxia-induced apoptosis in cardiomyocytes and protects cardiac cells during myocardial ischaemia,⁵⁰ and also prevents pancreatic β -cells from type 1 diabetes-induced apoptosis.⁵¹ Another compound, BIX (BiP Inducer X), is able to induce the expression of Grp78 through the ATF6 pathway.⁵² BIX has been shown to protect neuroblastoma cells from ER stress-induced cell death and to decrease infarct size in rodents following various models of cerebral ischaemia.^{52,53} However, none of these studies have investigated the precise localization of the protein.

Overall, we describe here for the first time a PERK-eIF2 α -negative feedback due to the activation of cell surface Grp78 by the serine protease tPA. We confirm the translocation of Grp78 from the ER to the neuronal surface, and we validate tPA as a ligand of Grp78. We demonstrate that tPA activation of cell surface Grp78 is capable to mediate beneficial effects on ER stress during cerebral ischaemia independently of its thrombolytic activity. Taken altogether, Grp78 represents an original therapeutic target to decrease the deleterious effects associated to ER stress.

Material and Methods

Reagents. Dulbecco's modified eagle's medium (DMEM), poly-D-lysine, cytosine β -D-arabinoside, fetal bovin serum, horse serum, D-glucose, trans-N,N'-1,4-Cyclohexanediybis[2-(4-chlorophenoxy)-acetamide (ISRIB), propidium iodide, tween-20, phosphatase inhibitor cocktail, protease inhibitor cocktail, guanabenz, Tris-HCl, NaCl, Triton-100X paraformaldehyde, sucrose, TRI reagent, hygromycin B, diisopropylethylamine (DIEA), piperidine, trifluoroacetic acid (TFA) and murine thrombin were from Sigma-Aldrich (Saint-Quentin-Fallavier, France). Beetle luciferin substrate was from Promega (Lyon, France). Glutamine, laminin, glucose-free DMEM, Roswell Park Memorial Institute 1640 medium (RPMI), MEM, Lipofectamine 2000, RIPA buffer, Pierce ECL Plus and M-MLV Reverse transcriptase were purchased from Fisher (Illkirch-Graffenstaden, France). AG1478 (N-(3-Chlorophenyl)-6,7-dimethoxy-4-quinazolinane hydrochloride) was purchased from Tocris (Bristol, UK). Bicinchoninic acid assay (BCA Protein Assay kit) was purchased from Pierce (Rockford, IL, USA). Human recombinant tPA (rtPA actilyse) was from Boehringer Ingelheim (Pacé, France). Human Receptor Associated Protein (RAP) was from Gentaur (Paris, France). 1,5-Dansyl-L-glutamyl-L-glycyl-L-arginine chloromethylketone (dGGACK) and Salubrinal were from Calbiochem (Nottingham, UK). Fmoc-L-amino acid residues were purchased from Senn Chemicals (Dielsdorf, Switzerland). The preloaded 4-hydroxymethyl-phenoxymethyl-copolystyrene-1%-divinylbenzene (HMP) resins and O-benzotriazol-1-yl-N,N,N',N'-tetramethyluronium hexafluorophosphate (HBTU) were purchased from Life Technologies (Villebon-sur-Yvette, France). Acetonitrile and N-methylpyrrolidone (NMP) were from Biosolve Chimie (Dieuze, France).

Thromboembolic model of stroke. Experiments were performed in accordance with French laws (act no. 87-848; Ministère de l'Agriculture et de la Forêt) and European Communities Council Directives of November 24, 1986 (86/609/EEC) guidelines, and have been approved by the local ethical committee. Experiments were performed following the ARRIVE guidelines (www.nc3rs.org.uk), including randomization and blind analyses. Mice were deeply anaesthetised with 5% isoflurane (Baxter, Paris, France, in a mixture of N₂O/O₂), placed in a stereotaxic device and maintained under anaesthesia for up to 2 h with 2% isoflurane in a 70/30 mixture of N₂O/O₂. Through a skin incision between the right eye and ear, the masseter muscle was excised, and a small craniotomy (diameter 1 mm) was performed on the parietal bone to expose the right middle cerebral artery. Thromboembolic stroke was induced as previously described.¹⁹ Briefly, craniotomy was performed by using cooled drill, then the dura was excised and a pipette filled with murine thrombin (1 U/ μ L) was directly inserted in the MCA lumen. One microliter of thrombin was injected to induce thrombus formation. Thrombolysis was induced by intravenous tPA (actilyse 10 mg/kg) administration (10% bolus, 90% over 40 min) 20 min after clot onset. Control animals received intravenous saline injection in the same conditions, and sham animals only had the surgical approach.

Bioluminescence imaging. CARE-Luciferase mice expressing the luciferase reporter gene under the control of the thymidine kinase promoter activated by two Trb3 (tribbles pseudokinase 3) sequences containing the three CARE (C/EBP (CCAAT/enhancer binding protein)—ATF response element) sequences of recognition (black circles on Supplementary Figure 3A) were previously described.¹⁸ Control experiments were performed after a local injection of tunicamycin (a well-known inducer of ER stress, 0.05 µg/g) in their abdomen. As expected, the luciferase signal measured 6 h after the injection of tunicamycin was increased by 20-fold when compared to control non-injected mice (representative images Supplementary Figure 3B and corresponding means Supplementary Figure 3C; *n* = 6; *P* < 0.01).

Post-stroke bioluminescence imaging was performed using the IVIS Spectrum (PerkinElmer, Villebon-sur-Yvette, France) imaging scanner coupled to the Living Image Software (PerkinElmer). Briefly, 100 mg/kg of *in vivo* luciferase substrate (beetle luciferin substrate, Promega) were injected intraperitoneally into each CARE-Luciferase mouse. Mice were then anaesthetised with isoflurane- and scanned 10 min after luciferin injection. The abdominal cavity was shaved to allow accurate collection of bioluminescence signals. Light emission was quantified with imaging software from constant regions of interest (ROI) drawn manually. Photon emission was measured as radiance in ps-1cm-2sr-1. The sensitivity of the imaging scanner was tested weekly with commercially available positive sources of bioluminescence. Excised brains were imaged immediately after euthanasia using the IVIS Spectrum (PerkinElmer) imaging scanner coupled to the Living Image software (PerkinElmer).

Luciferase biochemical assay. Luciferase assays were performed as previously described.⁵⁴ Luciferase activities measured in brain extracts were normalized to protein content (RLU/mg protein) and expressed as fold induction relative to the control condition.

Organotypic hippocampal slice cultures. Seven-day-old mouse pups of either sex were decapitated and their brain collected in PBS containing 5 mg of glucose. Hippocampal slices (400 µm) were prepared using a Mcllwain tissue chopper (Brinkmann Instruments, World Precision Instruments, Hitchin, UK) and placed on 0.4 µm Millicell culture inserts (Millipore, Guyancourt, France), as previously described.²⁴ Slices were maintained in a humidified incubator with 5% CO₂ at 37 °C with 1 ml of MEM containing 20% horse serum, supplemented with 10 mM HEPES and insulin, pH 7.2–7.3.

Neuronal cell cultures. Primary cultures of cortical neurones were prepared from foetal mice (embryonic day 14) as previously described.⁵⁵ Cells were cultured on individual glass bottom Petri dishes (MatTek Corporation, Ashland, MA, USA) or 24-well plates, previously coated with poly-D-lysine (0.1 mg/ml) and laminin (0.02 mg/ml), in DMEM supplemented with 5% foetal bovine serum, 5% horse serum and 1 mM glutamine. Cultures were maintained at 37 °C in a humidified 5% CO₂ atmosphere. Cytosine β-D-arabinoside (10 µM) was added after 3 days *in vitro* (DIV) to inhibit glial proliferation in the 24-well plates. Oxygen and glucose deprivation was performed after 11–12 DIV.

Oxygen and glucose deprivation (OGD). Hippocampal slices (7 DIV) or neuronal cultures (11–12 DIV) were subjected for various times to OGD in a hypoxic chamber (IN VIVO2 500; Ruskinn, AWEL International, Blain, France) programmed at 1% O₂, 5% CO₂ and 37 °C in glucose/serum-free deoxygenated DMEM. For reoxygenation, media were switched to oxygenated DMEM completed with D-glucose (4.5 mg/l) under normoxic conditions. Controls were subjected to sham washes.

Neuronal death. For hippocampal slices, neuronal death was assessed 24 h after reoxygenation by propidium iodide fluorescence. Propidium iodide (50 µg/µl) was added for 30 min in the medium, washed in PBS and then immersed in fixative buffer during 1 h (4% of paraformaldehyde in 0.1 M PBS, pH 7.4). Images were digitally captured using a Leica SP5 confocal microscope (Leica Microsystems SAS, Nanterre, France) and visualized with LAS AF lite software (Leica) and further quantified using ImageJ 1.45r software (National Institute of Health, Bethesda, MD, USA).

For cortical neurones, neuronal death was quantified 4 h after reoxygenation by measuring the lactate dehydrogenase activity released from damaged cells into the bathing medium with a cytotoxicity detection kit (Roche Diagnostics, Meylan, France).

Immunoblotting. Cells were dissociated in ice-cold TNT buffer (50 mM Tris-HCl pH 7.4; 150 mM NaCl; 0.5% Triton X-100; phosphatase and protease inhibitors cocktails) and centrifuged (12,000 g, 4 °C, 15 min). Protein concentration was measured by BCA Protein Assay method. Proteins (20 µg) were resolved on a 10% SDS-PAGE gel (Bio-rad, Marnes-la-Coquette, France) and transferred onto a polyvinylidene difluoride membrane. Membranes were blocked with PBS+0.1% tween-20, 5% milk and incubated overnight at 4 °C in blocking buffer containing primary antibodies. The following primary antibodies and dilutions were used: mouse anti-elf2α (1/1000; Cell Signaling L57A5; Ozyme, Montigny-le Bretonneux France), rabbit anti-Phospho-elf2α (1/1000 Cell Signaling 119A11), goat anti-TPA (1/1000; sc5239; Santa-Cruz, Heidelberg, Germany). Membranes were then incubated with the corresponding peroxidase-conjugated secondary antibodies (1/25000; Sigma-Aldrich) in blocking buffer, and visualized with an enhanced chemiluminescence Pierce ECL Plus kit.

Quantitative real-time PCR. Total RNA was isolated from neuronal culture with TRI reagent according to the manufacturer instructions. Total RNA was treated with TURBO DNase (Ambion, Saint Aubin, France) to avoid DNA contamination and quantified by spectrophotometry (NanoDrop Technologies, Wilmington, DE, USA). One µg of total RNA was reverse-transcribed by using the M-MLV Reverse transcriptase according to the manufacturer's instructions with the following cycle conditions: 42 °C (90 min); 85 °C (5 min). RT-qPCR was performed from 1:20 diluted cDNA in iQ SYBR Green Supermix (Bio-Rad; Marnes-la-Coquette, France) containing 500 nM of each primer. Based on mRNA-coding sequences (www.ensembl.org), mouse-specific primers were designed by using the Primer3Plus software (<http://www.bioinformatics.nl/cgi-bin/primer3plus/primer3plus.cgi>)⁵⁶ (sequences are in Table 1). Assays were run in triplicate on the CFX96 real-time system c1000 thermal cycler (Bio-Rad), with the following cycle conditions: 95 °C (3 min); (95 °C (2 s), 60 °C (20 s)) × 39; 70 °C (30 s). Normalization was performed according to the results of the geNorm analysis (QBase+ software, Biogazelle, Zwijnaarde, Belgium) (Supplementary Figure 4) as previously described.⁵⁷

Immunohistochemistry. Twenty-four hours after ischaemia mice were deeply anaesthetised and transcardially perfused with 0.9% NaCl heparinized followed by a mixture of 4% paraformaldehyde in 0.1 M PBS, pH 7.4 (150 ml). Brains were removed, washed in PBS buffer containing 20% sucrose and frozen in Tissue-Tek (Miles Scientific, Naperville, IL, USA). Coronal sections (10 µm) were cut on a cryostat (Leica CM3050, Leica Microsystems SAS), collected on poly-D-lysine slides, and stored at –80 °C. Sections were incubated overnight at room temperature with a goat anti-luciferase antibody (1/200; ab81823, Abcam, Cambridge, UK). The secondary F(ab')₂ coupled to fluorescein isothiocyanate (FITC; 1:600; Jackson ImmunoResearch, West Grove, PA, USA) was used for visualization under epifluorescence. Washed sections were coverslipped with

Table 1 qPCR primer sequences

Name	Primer (5'–3')	Forward (5'–3')
<i>ATF4</i>	TCCTGAACAGCGAAGTGTG	ACCCATGAGGTTTCAAGTGC
<i>CHOP</i>	CTGCCTTTCACCTTGGAGAC	CGTTTCTGGGGATGAGATA
<i>GADD34</i>	AGGACCCCGAGATTCCTCTA	CTTCGATCTCGTGCAAACTG
<i>Grp78</i>	ATAAACCCCGATGAGGCTGT	GGGGACAAACATCAAGCAGT
<i>ActinB</i>	GCAGCTCCTTCGTTGCCGGT	TACAGCCCGGGGAGCATCGT
<i>RPII3A</i>	TACGCTGTGAAGGCATCAAC	GGGAGGGGTTGGTATTCATC

Abbreviation: qPCR, quantitative PCR.

antifade medium containing DAPI. Sections were examined with a microscope (DM6000; Leica Microsystems SAS). Images were digitally captured using a camera (Flash 4.0, Hamamatsu, Iwata, Japan). Images were visualized with Metamorph software (Molecular Devices, Sunnyvale, CA, USA).

Immunocytochemistry. After a brief wash in PBS, neuronal cultures grown on glass bottom Petri dishes were fixed during 5 min in 0.1 M PBS containing 4% paraformaldehyde and 5% sucrose. After PBS washes, cells were blocked for 1 h in PBS-Tween 20 0.1% containing 1% BSA and then incubated overnight at 4 °C in blocking buffer containing primary antibodies (rabbit anti-Phospho-elf2 α ; 1/50; Cell Signaling #3597, Ozyme; mouse anti-NeuN (Fox3); 1/50; Millipore #MAB377). Primary antibodies were revealed using FITC-coupled secondary F(ab')₂ (1 : 600; Jackson ImmunoResearch). Confocal laser-scanning microscopy was performed using a Leica SP5 confocal microscope (Leica Microsystems SAS).

ER tracker. Cortical neurones in glass bottom Petri dishes at 11 DIV were loaded (30 min at 37 °C) with ER Tracker Blue (10 μ M Molecular Probes) before OGD, then washed with fresh serum-free DMEM and observed with LEICA SP5 confocal microscope (Leica Microsystems SAS), visualized with LAS AF lite software (Leica) and analysed with ImageJ 1.45r software (NIH) or Imaris software (Bitplane, Zurich, Switzerland).

Peptide synthesis. Grp78 (Leu⁹⁸-Leu¹¹⁵) (Grp78₍₉₈₋₁₁₅₎); LIGRTWNDPSVQG-DIKFL) and scramble (Grp78₍₉₈₋₁₁₅₎sc; GTNKSQDLWIPQLRDVFI) peptides were synthesized (0.1 mmol scale) on Fmoc-Leu-HMP and Fmoc-Ile-HMP resins, respectively, using an Applied Biosystems model 433A automatic peptide synthesizer (Life Technologies; Villebon-sur-Yvette, France) and the standard procedures, as previously described.^{58,59} All Fmoc-amino acids (1 mmol, 10 eq.) were coupled by *in situ* activation with HBTU (1.25 mmol, 12.5 eq.) and DIEA (2.5 mmol, 25 eq.) in NMP. Reactive side-chains were protected as follows: Arg, pentamethylidihydrobenzofuran (Pbf) sulfonamide; Asn and Gln, trityl (Trt) amide; Ser, Thr and Tyr, tert-butyl (tBu) ether; Asp and Glu, *O*-tert-butyl (OtBu) ester; Lys and Trp, tert-butyloxycarbonyl (Boc) carbamate. Peptides were deprotected and cleaved from the resin by trifluoroacetic acid (TFA) as previously described.⁶⁰ Crude peptides were purified by reversed-phase HPLC (RP-HPLC) on a Vydac 218TP1022 C18 column (2.2 \times 25 cm; Grace Discovery Sciences Alltech, Templemars, France) using a linear gradient (10–60% over 60 min for Grp78₍₉₈₋₁₁₅₎sc; 10–50% over 55 min for Grp78₍₉₈₋₁₁₅₎) of acetonitrile/TFA (99.9:0.1, v/v) at a flow rate of 10 ml/min. Peptides were analysed by RP-HPLC on a Vydac 218TP54 C18 column (0.46 \times 25 cm; Grace Discovery Sciences Alltech) using a linear gradient (10–60% over 25 min) of acetonitrile/TFA (99.9:0.1, v/v) at a flow rate of 1 ml/min. The purity of peptides was higher than 99.9%. Peptides were characterized by MALDI-TOF mass spectrometry on a Voyager DE-PRO (Applera, France) in the reflector mode with α -cyano-4-hydroxycinnamic acid as a matrix.

Production of radioactive tPA. A human tPA pcDNA5/FRT vector was constructed using a PCR strategy from the pUC19–HutPA vector kindly gifted by Prof. HR Lijnen and checked by automating sequencing. HEK-F1pIn cells (Life Technologies), grown in RPMI 1640 medium supplemented with 10% foetal bovine serum and 2 mM glutamine, were transfected with Lipofectamine 2000. Positive clones were isolated by hygromycin B selection. The quality of the transfection was assessed by quantitative RT-PCR. Transfected HEK cells were grown T300 flasks in the presence of radioactive medium mix (RPMI-1640 medium, 5% foetal bovine serum, 2 mM glutamine, EXPRESS Protein Labelling Mix containing 35S-methionine and 35S-cysteine) during 7 days. Radioactive tPA (tPA*) secreted in the supernatants was purified using a nickel-nitrilotriacetic acid metal-affinity chromatography matrix (Qiagen, Courtaboeuf, France). tPA* was then conditioned in HEPES buffer (0.35 M, pH 7.4) and stored at –20 °C. Immunoblottings to check tPA production were performed using a polyclonal sheep antiserum raised against human tPA (1:5000) prepared at the National Institute for agronomic research (INRA, Clermont-Theix, France), followed by incubation with the appropriate peroxidase-conjugated secondary antibody (Supplementary Figure 5A). Immunoblots were revealed with an enhanced chemoluminescence ECL Plus immunoblotting detection system (PerkinElmer-NEN, Paris, France). To ensure the incorporation of radioactivity, the blotting membrane was revealed by autoradiography by using Cyclone Imager (PerkinElmer) (Supplementary Figure 5B). Importantly, the procedure did not alter the enzymatic amidolytic activity of tPA*, as evidenced by a fluorogenic assay (Spectrofluor FL444, American Diagnostica, Neuville sur Oise, data not shown).

Immunoprecipitation. Cells were lysed in RIPA buffer and lysates were pre-cleared with goat IgG bound to 50% (v/v) Protein G-Sepharose for 1 h at 4 °C. Grp78 or tPA were immunoprecipitated overnight at 4 °C with specific antibodies pre-bound to protein G-sepharose (50% (v/v) protein G-sepharose plus 1 μ g of purified antibody at 4 °C for 2 h). The following day, immunocomplexes were washed four times with cold PBS and once with RIPA buffer. Immunocomplexes proteins were recovered in SDS-PAGE loading buffer by heating for 5 min at 90 °C, separated on 10% w/v gel and detected by western blot analysis using antibodies against Grp78 (goat anti-Grp78; 200 μ g/ml; Santa Cruz #SC1050).

tPA proteolytic activity assay. tPA* was incubated in the presence of a fluorogenic substrate (5 μ M) (Spectrofluor FL444, American Diagnostica). The reaction was carried out at 37 °C in 50 mM Tris (pH 8.0) containing 150 mM NaCl in a total volume of 100 μ l. The amidolytic activity was measured as the change in fluorescence emission at 440 nm (excitation at 360 nm).

Statistics. Mean \pm S.E.M. were represented on graphs, and analysed with the Mann–Whitney test (GraphPad Prism software).

Conflict of Interest

The authors declare no conflict of interest.

Acknowledgements. This project was supported by the Region Basse-Normandie and the AXA postdoctoral fellowship program, the INSERM, and the university of Caen. We thank Mr Gilbert Pigree and Mr Maxime Lemarchand for their help with the production of radioactive tPA (IMOGERE platform, University of Caen, France). Thanks to Dr Mario Gonzalez-Gronow for the gift of recombinant Grp78.

- Ron D, Walter P. Signal integration in the endoplasmic reticulum unfolded protein response. *Nat Rev Mol Cell Biol* 2007; **8**: 519–529.
- Walter P, Ron D. The unfolded protein response: from stress pathway to homeostatic regulation. *Science* 2011; **334**: 1081–1086.
- Szegezdi E, Logue SE, Gorman AM, Samali A. Mediators of endoplasmic reticulum stress-induced apoptosis. *EMBO Rep* 2006; **7**: 880–885.
- Roussel BD, Kruppa AJ, Miranda E, Crowther DC, Lomas DA, Marciniak SJ. Endoplasmic reticulum dysfunction in neurological disease. *Lancet Neurol* 2013; **12**: 105–118.
- Harding HP, Zhang Y, Ron D. Protein translation and folding are coupled by an endoplasmic-reticulum-resident kinase. *Nature* 1999; **397**: 271–274.
- Marciniak SJ, Garcia-Bonilla L, Hu J, Harding HP, Ron D. Activation-dependent substrate recruitment by the eukaryotic translation initiation factor 2 kinase PERK. *J Cell Biol* 2006; **172**: 201–209.
- Harding HP, Zhang Y, Zeng H, Novoa I, Lu PD, Calton M et al. An integrated stress response regulates amino acid metabolism and resistance to oxidative stress. *Mol Cell* 2003; **11**: 619–633.
- Marciniak SJ, Yun CY, Oyadomari S, Novoa I, Zhang Y, Jungreis R et al. CHOP induces death by promoting protein synthesis and oxidation in the stressed endoplasmic reticulum. *Genes Dev* 2004; **18**: 3066–3077.
- Mollereau B, Rzechorzek NM, Roussel BD, Sedru M, Van den Brink DM, Bailly-Maitre B et al. Adaptive preconditioning in neurological diseases - therapeutic insights from proteostatic perturbations. *Brain Res* 2016; **1648**: 603–616.
- Rissanen A, Sivenius J, Jolkonen J. Prolonged bihemispheric alterations in unfolded protein response related gene expression after experimental stroke. *Brain Res* 2006; **1087**: 60–66.
- Nakka VP, Gusain A, Raghuraj R. Endoplasmic reticulum stress plays critical role in brain damage after cerebral ischemia/reperfusion in rats. *Neurotox Res* 2010; **17**: 189–202.
- Szydlowska K, Tymianski M. Calcium, ischemia and excitotoxicity. *Cell Calcium* 2010; **47**: 122–129.
- Qi X, Okuma Y, Hosoi T, Nomura Y. Edaravone protects against hypoxia/ischemia-induced endoplasmic reticulum dysfunction. *J Pharmacol Exp Ther* 2004; **311**: 388–393.
- Tajiri S, Oyadomari S, Yano S, Morioka M, Gotoh T, Hamada JI et al. Ischemia-induced neuronal cell death is mediated by the endoplasmic reticulum stress pathway involving CHOP. *Cell Death Differ* 2004; **11**: 403–415.
- Hayashi T, Saito A, Okuno S, Ferrand-Drake M, Dodd RL, Chan PH. Damage to the endoplasmic reticulum and activation of apoptotic machinery by oxidative stress in ischemic neurons. *J Cereb Blood Flow Metab* 2005; **25**: 41–53.
- Paschen W, Hayashi T, Saito A, Chan PH. GADD34 protein levels increase after transient ischemia in the cortex but not in the CA1 subfield: implications for post-ischemic recovery of protein synthesis in ischemia-resistant cells. *J Neurochem* 2004; **90**: 694–701.
- McCaig D, Imai H, Gallagher L, Graham DI, Harland J, Moira Brown S et al. Evolution of GADD34 expression after focal cerebral ischaemia. *Brain Res* 2005; **1034**: 51–61.

18. Chaveroux C, Carraro V, Canaple L, Averous J, Maurin AC, Jousse C *et al*. *In vivo* imaging of the spatiotemporal activity of the eIF2 α -ATF4 signaling pathway: Insights into stress and related disorders. *Sci Signal* 2015; **8**: rs5.
19. Orset C, Macrez R, Young AR, Panthou D, Angles-Cano E, Maubert E *et al*. Mouse model of *in situ* thromboembolic stroke and reperfusion. *Stroke* 2007; **38**: 2771–2778.
20. Chevilly A, Lesept F, Lenoir S, Ali C, Parcq J, Vivien D. Impacts of tissue-type plasminogen activator (tPA) on neuronal survival. *Front Cell Neurosci* 2015; **9**: 415.
21. Yepes M. Tissue-type plasminogen activator is a neuroprotectant in the central nervous system. *Front Cell Neurosci* 2015; **9**: 304.
22. Yepes M, Roussel BD, Ali C, Vivien D. Tissue-type plasminogen activator in the ischemic brain: more than a thrombolytic. *Trends Neurosci* 2009; **32**: 48–55.
23. Correa F, Gauberti M, Parcq J, Macrez R, Hommet Y, Obiang P *et al*. Tissue plasminogen activator prevents white matter damage following stroke. *J Exp Med* 2011; **208**: 1229–1242.
24. Lemarchand E, Maubert E, Haelewyn B, Ali C, Rubio M, Vivien D. Stressed neurons protect themselves by a tissue-type plasminogen activator-mediated EGFR-dependent mechanism. *Cell Death Differ* 2015.
25. Zhang X, Polavarapu R, She H, Mao Z, Yepes M. Tissue-type plasminogen activator and the low-density lipoprotein receptor-related protein mediate cerebral ischemia-induced nuclear factor-kappaB pathway activation. *Am J Pathol* 2007; **171**: 1281–1290.
26. An J, Zhang C, Polavarapu R, Zhang X, Yepes M. Tissue-type plasminogen activator and the low-density lipoprotein receptor-related protein induce Akt phosphorylation in the ischemic brain. *Blood* 2008; **112**: 2787–2794.
27. Gonzalez-Gronow M, Selim MA, Pappas J, Pizzo SV. GRP78: a multifunctional receptor on the cell surface. *Antioxid Redox Signal* 2009; **11**: 2299–2306.
28. Tsai YL, Zhang Y, Tseng CC, Stanciuskas R, Pinaud F, Lee AS. Characterization and mechanism of stress-induced translocation of 78-kilodalton glucose-regulated protein (GRP78) to the cell surface. *J Biol Chem* 2015; **290**: 8049–8064.
29. Gonzalez-Gronow M, Gomez CF, de Ridder GG, Ray R, Pizzo SV. Binding of tissue-type plasminogen activator to the glucose-regulated protein 78 (GRP78) modulates plasminogen activation and promotes human neuroblastoma cell proliferation *in vitro*. *J Biol Chem* 2014; **289**: 25166–25176.
30. Kumar R, Azam S, Sullivan JM, Owen C, Cavener DR, Zhang P *et al*. Brain ischemia and reperfusion activates the eukaryotic initiation factor 2 α kinase, PERK. *J Neurochem* 2001; **77**: 1418–1421.
31. Owen CR, Kumar R, Zhang P, McGrath BC, Cavener DR, Krause GS. PERK is responsible for the increased phosphorylation of eIF2 α and the severe inhibition of protein synthesis after transient global brain ischemia. *J Neurochem* 2005; **94**: 1235–1242.
32. Zhang Y, Liu R, Ni M, Gill P, Lee AS. Cell surface relocation of the endoplasmic reticulum chaperone and unfolded protein response regulator GRP78/BiP. *J Biol Chem* 2010; **285**: 15065–15075.
33. Hardy B, Battler A, Weiss C, Kudasi O, Raiter A. Therapeutic angiogenesis of mouse hind limb ischemia by novel peptide activating GRP78 receptor on endothelial cells. *Biochem Pharmacol* 2008; **75**: 891–899.
34. Raiter A, Weiss C, Bechor Z, Ben-Dor I, Battler A, Kaplan B *et al*. Activation of GRP78 on endothelial cell membranes by an ADAM15-derived peptide induces angiogenesis. *J Vasc Res* 2010; **47**: 399–411.
35. Misra UK, Gonzalez-Gronow M, Gawdi G, Hart JP, Johnson CE, Pizzo SV. The role of Grp 78 in alpha 2-macroglobulin-induced signal transduction. Evidence from RNA interference that the low density lipoprotein receptor-related protein is associated with, but not necessary for, GRP 78-mediated signal transduction. *J Biol Chem* 2002; **277**: 42082–42087.
36. Gonzalez-Gronow M, Kaczowka SJ, Payne S, Wang F, Gawdi G, Pizzo SV. Plasminogen structural domains exhibit different functions when associated with cell surface GRP78 or the voltage-dependent anion channel. *J Biol Chem* 2007; **282**: 32811–32820.
37. Jindadamrongwech S, Thepparit C, Smith DR. Identification of GRP 78 (BiP) as a liver cell expressed receptor element for dengue virus serotype 2. *Arch Virol* 2004; **149**: 915–927.
38. Triantafyllou K, Fradelizi D, Wilson K, Triantafyllou M. GRP78, a coreceptor for coxsackievirus A9, interacts with major histocompatibility complex class I molecules which mediate virus internalization. *J Virol* 2002; **76**: 633–643.
39. Goldenberg-Cohen N, Raiter A, Gaydar V, Dratviman-Storobinsky O, Goldstein T, Weizman A *et al*. Peptide-binding GRP78 protects neurons from hypoxia-induced apoptosis. *Apoptosis* 2012; **17**: 278–288.
40. Tissue plasminogen activator for acute ischemic stroke. The National Institute of Neurological Disorders and Stroke rt-PA Stroke Study Group. *N Engl J Med* 1995; **333**: 1581–1587.
41. Kim JT, Fonarow GC, Smith EE, Reeves MJ, Navalkele DD, Grotta JC *et al*. Treatment with tPA in the "Golden Hour" and the shape of the 4.5 hour time-benefit curve in the National US Get With The Guidelines-Stroke Population. *Circulation* 2016; **135**: 128–139.
42. Tsirka SE, Gualandris A, Amaral DG, Strickland S. Excitotoxin-induced neuronal degeneration and seizure are mediated by tissue plasminogen activator. *Nature* 1995; **377**: 340–344.
43. Nicole O, Docagne F, Ali C, Margail I, Carmeliet P, MacKenzie ET *et al*. The proteolytic activity of tissue-plasminogen activator enhances NMDA receptor-mediated signaling. *Nat Med* 2001; **7**: 59–64.
44. Liot G, Roussel BD, Lebeurrier N, Benchenane K, Lopez-Atalaya JP, Vivien D *et al*. Tissue-type plasminogen activator rescues neurones from serum deprivation-induced apoptosis through a mechanism independent of its proteolytic activity. *J Neurochem* 2006; **98**: 1458–1464.
45. Parcq J, Bertrand T, Montagne A, Baron AF, Macrez R, Billard JM *et al*. Unveiling an exceptional zymogen: the single-chain form of tPA is a selective activator of NMDA receptor-dependent signaling and neurotoxicity. *Cell Death Differ* 2012; **19**: 1983–1991.
46. Wu F, Nicholson AD, Haile WB, Torre E, An J, Chen C *et al*. Tissue-type plasminogen activator mediates neuronal detection and adaptation to metabolic stress. *J Cereb Blood Flow Metab* 2013; **33**: 1761–1769.
47. Wu F, Echeverry R, Wu J, An J, Haile WB, Cooper DS *et al*. Tissue-type plasminogen activator protects neurons from excitotoxin-induced cell death via activation of the ERK1/2-CREB-ATF3 signaling pathway. *Mol Cell Neurosci* 2013; **52**: 9–19.
48. Wang YF, Tsirka SE, Strickland S, Stieg PE, Soriano SG, Lipton SA. Tissue plasminogen activator (tPA) increases neuronal damage after focal cerebral ischemia in wild-type and tPA-deficient mice. *Nat Med* 1998; **4**: 228–231.
49. Lesept F, Chevilly A, Jezequel J, Ladepeche L, Macrez R, Aimable M *et al*. Tissue-type plasminogen activator controls neuronal death by raising surface dynamics of extrasynaptic NMDA receptors. *Cell Death Dis* 2016; **7**: e2466.
50. Hardy B, Raiter A. Peptide-binding heat shock protein GRP78 protects cardiomyocytes from hypoxia-induced apoptosis. *J Mol Med (Berl)* 2010; **88**: 1157–1167.
51. Raiter A, Tenenbaum A, Yackobovitch-Gavan M, Battler A, Hardy B. Peptide binding glucose regulated protein 78 improves type 1 diabetes by preventing pancreatic beta cell apoptosis. *Exp Clin Endocrinol Diabetes* 2016; **124**: 239–245.
52. Kudo T, Kanemoto S, Hara H, Morimoto N, Morihara T, Kimura R *et al*. A molecular chaperone inducer protects neurons from ER stress. *Cell Death Differ* 2008; **15**: 364–375.
53. Oida Y, Hamanaka J, Hyakkoku K, Shimazawa M, Kudo T, Imaizumi K *et al*. Post-treatment of a BiP inducer prevents cell death after middle cerebral artery occlusion in mice. *Neurosci Lett* 2010; **484**: 43–46.
54. B'Chir W, Maurin AC, Carraro V, Averous J, Jousse C, Muranishi Y *et al*. The eIF2 α /ATF4 pathway is essential for stress-induced autophagy gene expression. *Nucleic Acids Res* 2013; **41**: 7683–7699.
55. Baron A, Montagne A, Casse F, Launay S, Maubert E, Ali C *et al*. NR2D-containing NMDA receptors mediate tissue plasminogen activator-promoted neuronal excitotoxicity. *Cell Death Differ* 2010; **17**: 860–871.
56. Rozen S, Skaletsky H. Primer3 on the WWW for general users and for biologist programmers. *Methods Mol Biol* 2000; **132**: 365–386.
57. Bruckert G, Vivien D, Docagne F, Roussel BD. Normalization of reverse transcription quantitative PCR data during ageing in distinct cerebral structures. *Mol Neurobiol* 2015; **53**: 1540–1550.
58. Leprince J, Gandolfo P, Thoumas JL, Patte C, Fauchere JL, Vaudry H *et al*. Structure-activity relationships of a series of analogues of the octadecaneuropeptide ODN on calcium mobilization in rat astrocytes. *J Med Chem* 1998; **41**: 4433–4438.
59. Leprince J, Oulyadi H, Vaudry D, Masmoudi O, Gandolfo P, Patte C *et al*. Synthesis, conformational analysis and biological activity of cyclic analogs of the octadecaneuropeptide ODN. Design of a potent endozepine antagonist. *Eur J Biochem* 2001; **268**: 6045–6057.
60. Chatenet D, Dubessy C, Boularan C, Scalbert E, Pfeiffer B, Renard P *et al*. Structure-activity relationships of a novel series of urotensin II analogues: identification of a urotensin II antagonist. *J Med Chem* 2006; **49**: 7234–7238.

Supplementary Information accompanies this paper on Cell Death and Differentiation website (<http://www.nature.com/cdd>)